

Defect physics in Yb³⁺-doped CaF₂ from first-principles calculation

Yun-Hyok Kye^a, Chol-Jun Yu^{*a}, Un-Gi Jong^a, Chol-Nam Sin^a, Weiping Qin^b

^aChair of Computational Materials Design, Faculty of Materials Science, Kim Il Sung University, Ryongnam-Dong, Taesong District, Pyongyang, Democratic People's Republic of Korea

^bState Key Laboratory on Integrated Optoelectronics, College of Electronic Science and Engineering, Jilin University, Changchun, Jilin 130012, China

Abstract

Calcium fluoride has been widely used for light up-/down-conversion luminescence by accommodating lanthanide ions as sensitizers or activators. Especially, Yb-doped CaF₂ exhibits unique defect physics, causing various effects on the luminescence. This makes it vital for high efficiency of devices to control the defect-clustering, but theoretically principal guidelines for this are rarely provided. Here we perform the first-principles study on defect physics in Yb-doped CaF₂ to reveal the thermodynamic transition levels and formation energies of possible defects. We suggest that the fluorine rich growth condition can play a key role in enhancing the luminescence efficiency by facilitating the Yb-clustering and suppressing the defect quenchers in bulk. Detailed energetics of defect aggregation not only well explains the experimentally favored Yb-clustering but also presents *n*- or *p*-type doping method for the cluster control.

Recently, lanthanide (Ln) doped nanophosphors have attracted a great interest due to their appealing applications on photodynamic therapy, sensing, solar cell devices and so on [1, 2, 3, 4, 5]. Among various Ln hosting materials, fluorides have been paid much attention for their low phonon energies, excellent photochemical stability and low cytotoxicity [6, 7, 8]. In particular, calcium fluoride (CaF₂) is one of the most intensively studied host for phosphors with interesting Ln-dopant clustering and up/down-conversion luminescent properties [9, 10, 11, 12].

Trivalent ytterbium ion (Yb³⁺) is a typical Ln-dopant for CaF₂, used as a sensitizer for up-conversion (UC) [13, 14, 15, 16] while an activator for down-conversion (DC) processes [17, 18]. In the CaF₂ host, Yb³⁺ ions are prone to form clusters such as dimer, trimer, tetramer and hexamer, which enlarge the absorption and emission bands being beneficial to the efficient cooperative and non-cooperative sensitization [19, 20]. Moreover, due to a single long-lived excited state of ²F_{5/2}, the Yb³⁺ ions hardly suffer from the cross relaxation [21, 22, 23], although other Ln-clusters often show optical losses due to the cross-relaxation. In order to reveal the mechanism of such Ln clustering in CaF₂, many theoretical works have been reported [9, 24], but yet a precise quantitative calculation of defect energetics at the level of quantum theory is not provided.

In this study, we investigate the defect physics of Yb-doped CaF₂ by using density functional theory (DFT) calculations. We make modeling of point and pair defects using the supercells, and calculate their formation energies and thermodynamic transition levels under the different growth conditions. The ground and optically excited states of Yb³⁺ ion are shown to be placed between the valence band maximum (VBM) and

the conduction band minimum (CBM) of the host CaF₂, giving rise to the deep trap states for charge carriers being adverse to the efficient luminescence. Through the analysis of defect energetics, we find that the F-rich (or Ca-poor) growth condition is favorable for suppressing the defects with deep trap states and for promoting the advantageous clustering of Yb-dopants. Based on the results, we also suggest that *n*- or *p*-type doping can be used to manage the clustering of Ln-dopants.

All the calculations were performed by using the projector augmented wave method as implemented in the Quantum ESPRESSO code [25]. The configurations of valence electrons are Ca-3s²3p⁶4s², F-2s²2p⁵, and Yb-5s²5p⁶4f¹⁴6s², emphasizing the direct use of *f* electrons in Yb element, and the scalar relativistic corrections were considered for the ionic cores. The cutoff energies were set to be 40 and 400 Ry for wave function and electron density, respectively. The special *k*-points were set to be Γ -centered (8 × 8 × 8) and (2 × 2 × 2) for CaF₂ unit-cell (space group *Fm* $\bar{3}$ *m*, 12 atoms, see Fig. 1a) and Yb-doped CaF₂ 2 × 2 × 2 supercell (96 atoms, see Fig. 1b). Atoms were relaxed until the forces converged to 5 × 10⁻⁵ Ry/Bohr with the PBEsol functional [26]. After atomic relaxation, the DFT total energies were refined using the hybrid HSE06 functional [27] with 50% nonlocal Hartree-Fock exchange addition, considering the underestimation of CaF₂ band gap at the level of generalized gradient approximation (GGA) and the severe self-interaction error (SIE) of Yb 4*f* orbitals [28, 29]. In the calculation of defect formation energy, the finite size effects were corrected by using the calculated static dielectric constant of 8.0 and deeplying Ca-3s level for the potential alignment [30, 31].

The lattice constant of CaF₂ unit-cell was determined to be 5.40 Å in good agreement with the experimental value of 5.45 Å [32]. As expected, the band gap was underestimated to be 7.33 eV with PBEsol-GGA, and widened to be 10.19 eV with hybrid HSE06, being closer to the experimental value of

*Corresponding author

Email address: cj.yu@ryongnamsan.edu.kp (Chol-Jun Yu)

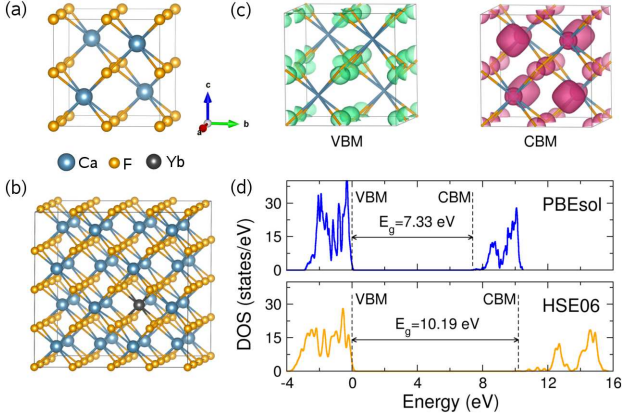


Figure 1: (a) Crystal structure of CaF₂ unit cell and (b) 2 × 2 × 2 supercell containing antisite defect Yb_{Ca}. (c) Isosurface plot of charge densities corresponding to the valence band maximum (VBM) and the conduction band minimum (CBM). (d) Density of states (DOS) in CaF₂ unit cell with different band gaps E_g from PBEsol and HSE06 functionals.

11.80 eV [33] (see Fig. 1d). With the optimized unit cell parameters, we built the 2×2×2 supercells, and made the point defects including interstitials (Ca_i, F_i, Yb_i), vacancies (V_{Ca}, V_F) and antisite (Yb_{Ca}) and pair defects (Yb_i-F_i, Yb_{Ca}-F_i, Yb_{Ca}-2F_i, 2(Yb_{Ca}-F_i)) in it (see Figs. S1 and S2). Possible charge states were assigned to the defects. Here, Yb_{Ca}-F_i and 2(Yb_{Ca}-F_i) were devised to represent the experimentally observed Yb monomer and dimer in line with the Catlow's former theoretical work [9]. Note that although the Yb³⁺ dopants were thought to substitute the Ca²⁺ ions, we also simulate the interstitial defect Yb_i, which is likely to form under the proper environmental condition.

First, we evaluated the thermodynamic transition levels between the different charge states q_1 and q_2 of defect D by applying the following equation [30, 34],

$$\varepsilon(q_1/q_2) = \frac{E[D^{q_1}] + E_{\text{corr}}[D^{q_1}] - E[D^{q_2}] - E_{\text{corr}}[D^{q_2}]}{q_2 - q_1} \quad (1)$$

where $E[D^q]$ is the DFT total energy of the supercell containing the defect with charge state D^q and $E_{\text{corr}}[D^q]$ is the correction term for the finite size effect of supercell and defect-induced electrostatic potential shift [30]. Figure 2 shows the thermodynamic transition levels for the point and pair defects calculated by both PBEsol and HSE06 functionals. When using the hybrid HSE06 functional, VBM is shifted downward by 2.03 eV being similar to the former calculation of 1.80 eV with the hybrid PBE0 [35], while CBM is shifted upward by 0.83 eV. We see that in the PBEsol calculation all the native point defects have deep transition levels in the region between VBM and CBM, whereas in HSE06 calculation most of the transition levels move towards the band edges becoming shallower, except the V_F defect.

In order to determine which levels can trap excited $4f$ electrons of Yb³⁺ ions during the energy transferring process, we correlate the Fermi energy of defective supercells containing nominally charged Yb³⁺ ion to the ground ²F_{7/2} level of Yb³⁺ [36]. The Fermi energies were estimated to be 1.03 eV

and 2.76 eV above VBMs for PBEsol and HSE06 respectively (see Table S2). Then, the level of the optically excited state ²F_{5/2} of Yb³⁺ can be found at 1.26 eV (corresponding to 980 nm excitation energy) over this level, as denoted by yellow color in Fig. 2. When compared HSE06 calculation to the PBEsol, the transition levels are separated further from the ²F_{5/2} level, indicating that only the hybrid functional can ensure the effective role of CaF₂ in the UC/DC luminescence. In the HSE06 calculation, the point defect Yb_{Ca} and the pair defect Yb_i-F_i are found to cause electron trap readily via non-radiative relaxation of absorbing one or two photons, due to their transition levels $\varepsilon(1+/0)$ and $\varepsilon(2+/1+)$ close to the ²F_{5/2} level. For the efficient energy transfer from CaF₂ host to Yb³⁺ ions, they should be suppressed.

Next, we calculated the formation energies of defects to examine their formation possibility. The chemical potentials of species μ_i can be changeable according to the synthesis condition, and thus have the values between its lower (poor condition) and upper (rich condition) limits [30]. We refer the rich conditions of Ca and F species to the fcc-metal bulk and gas states respectively, using the DFT total energies per atom. In thermodynamic equilibrium growth conditions, the existence of CaF₂ should satisfy $\mu_{\text{Ca}} + 2\mu_{\text{F}} = \mu_{\text{CaF}_2}$, where μ_{CaF_2} is approximated to be the DFT total energy per formula unit of CaF₂ unit cell, giving the constraint for the chemical potentials and their lower limits as $\mu_{\text{Ca}}^{\text{poor}} = \mu_{\text{CaF}_2} - \mu_{\text{F}}^{\text{rich}}$, $\mu_{\text{F}}^{\text{poor}} = \mu_{\text{CaF}_2} - \mu_{\text{Ca}}^{\text{rich}}$. The relative differences between the lower and upper limits, $\Delta\mu_i = \mu_i^{\text{poor}} - \mu_i^{\text{rich}}$, were calculated to be -13.10 eV for Ca and -6.55 eV for F respectively. For the extrinsic Yb dopant, besides the upper constraint from the metal bulk energy, another constraint exists as $\mu_{\text{Yb}} + 3\mu_{\text{F}} \leq \mu_{\text{YbF}_3}$, which prevents the formation of secondary phase and sets up the upper limit of μ_{Yb} according to the rich or poor condition of host elements. Considering these two upper constraints, the difference between the chemical potentials for the F-rich and -poor conditions was obtained to be -14.04 eV.

Figure 3 shows the formation energy diagrams of the relevant defects under the F-rich (Ca-poor) and F-poor (Ca-rich) conditions. Under the F-rich condition, V_{Ca}²⁻ is found to be the dominant defect with the lowest formation energy in the most range of E_{F} , while under the F-poor condition the point defect Ca_F²⁺ is dominant. Fortunately, these defects are not likely to create deep trap states. Our major concern is the Yb-doped point defects. Under the both conditions, Yb is in the possibly rich conditions as mentioned above, which, otherwise, can seem to be relatively poor in F-rich condition and relatively rich in F-poor condition. Meanwhile, for the lower Yb concentrations, the formation energy diagrams of Yb-doped defects can be expected to move upwards. As shown in Fig. 3, the antisite Yb_{Ca}, which was found to generate deep trap states, has the formation energy bigger than 1 eV under any thermodynamically reasonable condition. This is contradictory to the experimental results of high Yb-doping concentration [6] and so we conclude that Yb_{Ca} defect can be feasibly formed only by the influence of the intrinsic defect F_i¹⁻. On the other hand, the formation energy of interstitial Yb dopant (Yb_i) was found to be much higher on the whole span of E_{F} under the F-rich condition but lower be-

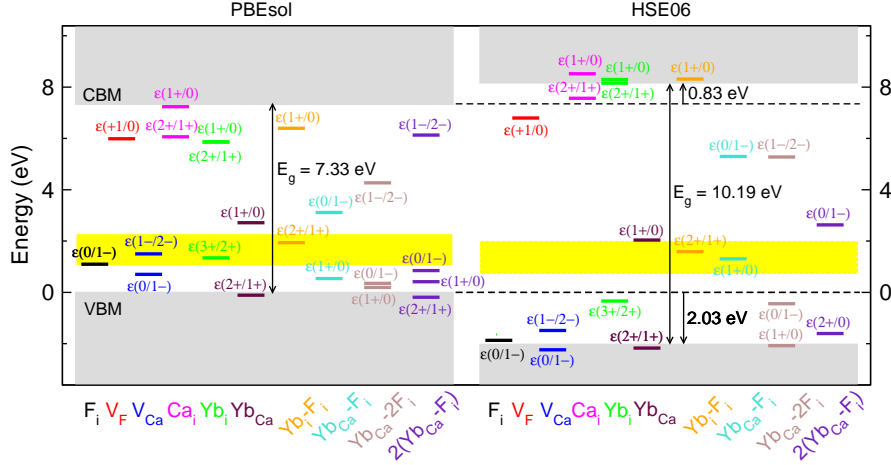


Figure 2: Thermodynamic transition levels of point and pair defects in Yb-doped CaF_2 calculated with PBEsol (left) and HSE06 (right) functionals. Bands are aligned with respect to their electrostatic potentials. Yellow regions represent the Fermi energy values between the ground ($^2F_{7/2}$) and optically excited ($^2F_{5/2}$) levels of Yb^{3+} ion.

low $E_F = 6.64$ eV under the F-poor condition than that of Yb_{Ca} . Providing that Yb_{Ca} is easily transformed to the pair defects like $\text{Yb}_{\text{Ca}}\text{-F}_i$, we can introduce the F-rich condition to suppress the formation of Yb_i and the undesirable pair defect $\text{Yb}_i\text{-F}_i$.

In order to check the probability of pair defect formation, we estimated their binding energies, defined as $E_b = H_f[A] + H_f[B] - H_f[AB]$ [30], where $H_f[A]$ is the formation energy of

point defect A and $H_f[AB]$ is that of pair defect. For the complex defects composed of more than three components such as $\text{Yb}_{\text{Ca}}\text{-2F}_i$ and $2(\text{Yb}_{\text{Ca}}\text{-F}_i)$, the pair defect $\text{Yb}_{\text{Ca}}\text{-F}_i$ was adopted as a reactant, and for the latter case two possible reaction pathways were considered; Route1: $\text{Yb}_{\text{Ca}}\text{-F}_i + \text{Yb}_{\text{Ca}}\text{-F}_i \rightarrow 2(\text{Yb}_{\text{Ca}}\text{-F}_i)$ and Route2: $\text{Yb}_{\text{Ca}}\text{-2F}_i + \text{Yb}_{\text{Ca}} \rightarrow 2(\text{Yb}_{\text{Ca}}\text{-F}_i)$. Figure 4 shows the calculated binding energies of the relevant pair defects. Positive binding energy indicates the stable aggregation of defects and parallel parts of lines to the Fermi energy axis represent the charge equality of reactants and products. Via the route of $\text{Yb}_{\text{Ca}}^{1+} + \text{F}_i^{1-} \rightarrow [\text{Yb}_{\text{Ca}}\text{-F}_i]^0$ around $E_F = 3.5$ eV, $\text{Yb}_{\text{Ca}}\text{-F}_i$ has the positive binding energy of 0.68 eV, and for $\text{Yb}_{\text{Ca}}\text{-F}_i$, the route $\text{Yb}_i^{3+} + \text{F}_i^{1-} \rightarrow [\text{Yb}_i\text{-F}_i]^{2+}$ yields the binding energy of 1.93 eV around $E_F = 1$ eV. Two routes for the formation of $2(\text{Yb}_{\text{Ca}}\text{-F}_i)$ from $[\text{Yb}_{\text{Ca}}\text{-F}_i]^0$ also verify the exothermic binding reaction as early suggested by Catlow's calculation [9] and elucidate the origins of experimentally observed Yb-clustering even at low concentration [11, 12]. Positive binding energies of $\text{Yb}_i\text{-2F}_i$, $\text{Yb}_{\text{Ca}}\text{-2F}_i$ and $2(\text{Yb}_{\text{Ca}}\text{-F}_i)$ indicate a facile aggregation of isolated Yb_{Ca} with F_i and guarantee the rare existence of this kind of trap defects. Meanwhile, another quenching candidate $\text{Yb}_i\text{-F}_i$ can be favorably formed due to the positive binding energy through the whole E_F range, requiring an induction of the F-rich condition for the high luminescence efficiency as mentioned above.

Finally, we turn our attention to the binding energy variation of complex defects in relation with the Fermi energy. In Fig. 4, it is noticeable that binding energy of $\text{Yb}_{\text{Ca}}\text{-F}_i$ decreases to a negative value of -2.57 eV as E_F approaching to CBM. Dimer binding energy in Route2 also shows a decreasing trend to the negative value near CBM, while that in Route1 is -1.77 eV near VBM. Aggregation of F_i and $\text{Yb}_{\text{Ca}}\text{-F}_i$ to $\text{Yb}_{\text{Ca}}\text{-2F}_i$ is not likely to occur around VBM because of its lower binding energy in the vicinity of zero. In principle, this degradable behavior near the band edges is mainly originated in the different charge states of Yb and F dopants from their nominal values. It is well accepted that the driving force of Yb-clustering is Coulomb interaction between $\text{Yb}_{\text{Ca}}^{1+}$ and F_i^{1-} , but stabilized neutral states of Yb_{Ca}^0 and

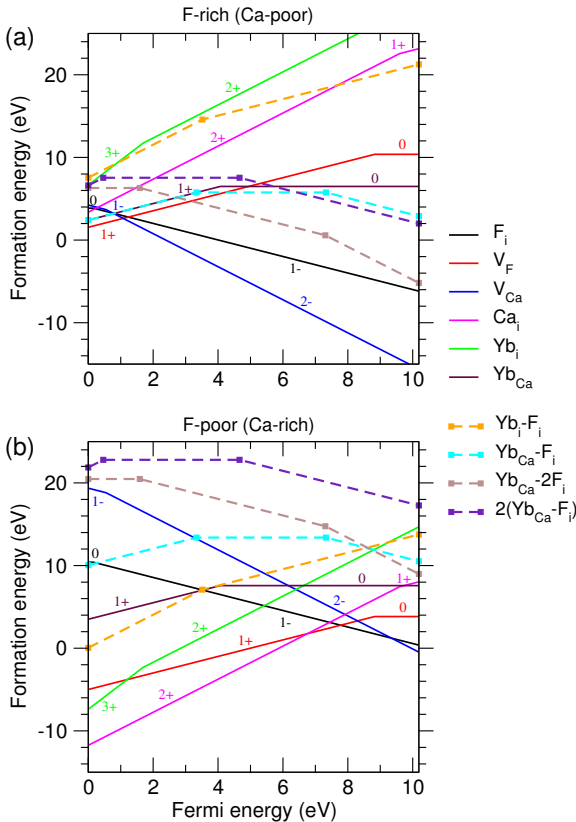


Figure 3: Defect formation energy diagrams under (a) F-rich (Ca-poor) and (b) F-poor (Ca-rich) conditions as a function of Fermi energy.

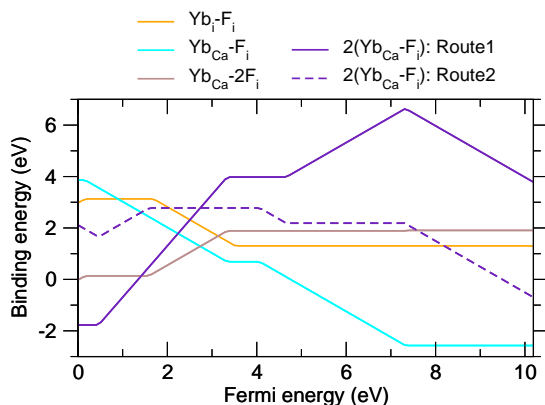


Figure 4: Binding energies of pair defects from their component point defects as a function of Fermi energy.

F_i^0 impede the defect aggregation. For this reason, we recommend extrinsic or intrinsic p/n -type doping for controlling the Yb-clustering. We can deduce that segregation product of p -type doping through the inverse process of Route1 is $Yb_{Ca}-F_i$, while n -type doping results in $Yb_{Ca}-2F_i$ following the inverse reaction of Route2.

In summary, we have investigated the defect physics of Yb-doped CaF_2 to reveal thermodynamic transition levels and defect formation energies by using DFT calculations. Multielectronic levels of Yb^{3+} ion for the optical spectra ($^2F_{7/2}$ and $^2F_{5/2}$) were presumably determined in relation with the DFT electronic structure, and Yb_{Ca} and Yb_i-F_i were thought to be bulk energy quenchers with deep trap levels. Under the F-rich growth condition, both trap defects can be suppressed due to the low concentration of Yb_i and the dimerization of Yb_{Ca} . Experimentally observed Yb-clustering effect was explained by the positive binding energies of defects, but n - or p -type doping provided negative effects on the aggregation. Although further study on the binding mechanism between Yb and other Ln-dopants are needed, our study can provide a guidance for tuning of Ln-clustering in CaF_2 for efficient UC/DC luminescence.

Acknowledgments

This work was supported partially by the State Committee of Science and Technology, Democratic People's Republic of Korea. The calculations have been performed on the HP Blade System C7000 (HP BL460c) that is owned and managed by the Faculty of Materials Science, Kim Il Sung University.

Appendix A. Supplementary data

Supplementary data related to this article can be found at URL.

Notes

The authors declare no competing financial interest.

References

- [1] L. Huang, T. Yamashita, R. Jose, Y. Arai, T. Suzuki, Y. Ohishi, Intense ultraviolet emission from Tb^{3+} and Yb^{3+} codoped glass ceramic containing CaF_2 nanocrystals, *Appl. Phys. Lett.* 90 (2007) 131116.
- [2] A. Bagheri, H. Arandiyani, C. Boyer, M. Lim, Lanthanide-doped upconversion nanoparticles: emerging intelligent light-activated drug delivery systems, *Adv. Sci.* 3 (2016) 1500437.
- [3] X. Ai, C. J. H. Ho, J. Aw, A. B. E. Attia, J. Mu, Y. Wang, X. Wang, Y. Wang, X. Liu, H. Chen, M. Gao, X. Chen, E. K. L. Yeow, G. Liu, M. Olivo, B. Xing, *In vivo* covalent cross-linking of photon-converted rare-earth nanostructures for tumour localization and theranostics, *Nat. Commun.* 7 (2016) 10432.
- [4] Y.-T. Wong, S.-Y. Pang, M.-K. Tsang, Y. Liu, H. Huang, S.-F. Yu, J. Hao, Electrochemically assisted flexible lanthanide upconversion luminescence sensing of heavy metal contamination with high sensitivity and selectivity, *Nanoscale Adv.* 1 (2019) 265–272.
- [5] X. Huang, S. Han, W. Huang, X. Liu, Enhancing solar cell efficiency: the search for luminescent materials as spectral converters, *Chem. Soc. Rev.* 42 (2013) 173–201.
- [6] B. Zhou, L. Tao, Y. H. Tsang, W. Jin, Coreshell nanoarchitecture: a strategy to significantly enhance white-light upconversion of lanthanide-doped nanoparticles, *J. Mater. Chem. C* 1 (2013) 4313–4318.
- [7] Y. Li, Y. Zhou, X. Li, J. Sun, Z. Ren, W. Wen, X. Yang, G. Hana, A facile approach to upconversion crystalline $CaF_2:Yb^{3+}, Tm^{3+}/mSiO_2$ nanospheres for tumor therapy, *RSC Adv.* 6 (2016) 38365.
- [8] K. Prorok, A. Bednarkiewicz, B. Cichy, A. Gnach, M. Misiak, M. Sobczyk, W. Strek, The impact of shell host ($NaYF_4/CaF_2$) and shell deposition methods on the up-conversion enhancement in Tb^{3+} , Yb^{3+} codoped colloidal α - $NaYF_4$ core-shell nanoparticles, *Nanoscale* 6 (2014) 1855–1864.
- [9] J. Corish, C. R. A. Catlow, P. W. M. Jacobs, S. H. Ong, Defect aggregation in anion-excess fluorites. Dopant monomers and dimers, *Phys. Rev. B* 25 (1982) 6425–6438.
- [10] R. H. Petit, P. Evesque, J. Duran, Dimers and clusters in $CaF_2:Pr^{3+}$. Laser selective excitation and time-resolved spectroscopy, *J. Phys. C: Solid State Phys.* 14 (1981) 5081–5090.
- [11] V. Petit, P. Camy, J.-L. Doualan, X. Portier, R. Moncorgé, Spectroscopy of $Yb^{3+}:CaF_2$: From isolated centers to clusters, *Phys. Rev. B* 78 (2008) 085131.
- [12] A. Lyberis, A. J. Stevenson, A. Suganuma, S. Ricaud, F. Druon, F. Herbst, D. Vivien, P. Gredin, M. Mortier, Effect of Yb^{3+} concentration on optical properties of $Yb:CaF_2$ transparent ceramics, *Optical Materials* 34 (2012) 965–968.
- [13] T. Aidilibike, J. Guo, L. Wang, X. Liu, Y. Lia, W. Qin, Ultraviolet upconversion emission of Pb^{2+} ions sensitized by Yb^{3+} -trimers in CaF_2 , *RSC Adv.* 7 (2017) 2676–2681.
- [14] Y. Li, J. Guo, X. Liu, T. Aidilibike, W. Qin, White upconversion luminescence in $CaF_2: Yb^{3+}/Eu^{3+}$ powders via incorporating Y^{3+} ions, *Phys. Chem. Chem. Phys.* 18 (2016) 16094–16097.
- [15] Y. Li, J. Guo, X. Liu, T. Aidilibike, W. Qin, Pure red upconversion emission from $CaF_2: Yb^{3+}/Eu^{3+}$, *J. Lumin* 185 (2017) 247–250.
- [16] H. Dong, L.-D. Sun, C.-H. Yan, Basic understanding of the lanthanide related upconversion emissions, *Nanoscale* 5 (2013) 5703–5714.
- [17] P. Molina, V. Vasyliov, E. G. Vllora, K. Shimamura, $Tb^{3+}-Yb^{3+}$ cooperative down and up conversion processes in $Tb_{0.81}Ca_{0.19}F_{2.81}:Yb^{3+}$ single crystals, *J. Appl. Phys.* 110 (2011) 123527.
- [18] J. T. van Wijngaarden, S. Scheidelaar, T. J. H. Vlugt, M. F. Reid, A. Meijerink, Energy transfer mechanism for downconversion in the (Pr^{3+} , Yb^{3+}) couple, *Phys. Rev. B* 81 (2010) 155112.
- [19] S. Ricaud, F. Druon, D. N. Papadopoulos, A. Pellegrina, F. Balembois, P. Georges, A. Courjaud, P. Camy, J. L. Doualan, R. Moncorgé, High-power diode-pumped cryogenically cooled $Yb:CaF_2$ laser with extremely low quantum defects, *Opt. Lett.* 36 (2011) 1602–1604.
- [20] D. Serrano, A. Braud, J. L. Doualan, P. Camy, R. Moncorgé, Pr^{3+} cluster management in CaF_2 by codoping with Lu^{3+} or Yb^{3+} for visible lasers and quantum down-converters, *J. Opt. Soc. Am. B* 29 (2012) 1854–1862.
- [21] G. Chen, C. Yang, P. N. Prasad, Nanophotonics and Nanochemistry: Controlling the Excitation Dynamics for Frequency Up- and Down-Conversion in Lanthanide-Doped Nanoparticles, *Acc. Chem. Res.* 46 (2013) 1474–1486.

- [22] C. Chen, C. Li, Z. Shi, Current Advances in Lanthanide-Doped Upconversion Nanostructures for Detection and Bioapplication, *Adv. Sci.* 3 (2016) 1600029.
- [23] D. Serrano, A. Braud, J.-L. Doualan, P. Camy, R. Moncorgé, Highly efficient energy transfer in Pr^{3+} , Yb^{3+} codoped CaF_2 for luminescent solar converters, *J. Opt. Soc. Am. B* 28 (2011) 1760–1765.
- [24] P. J. Bendall, C. R. A. Catlow, J. Corish, P. W. M. Jacobs, Defect aggregation in anion-excess fluorites II. Clusters containing more than two impurity atoms., *J. Solid State Chem.* 51 (1984) 159.
- [25] P. Giannozzi and S. Baroni and N. Bonini and M. Calandra and R. Car, et al., QUANTUM ESPRESSO: a modular and open-source software project for quantum simulations of materials, *J. Phys.:Condens. Matter* 21 (2009) 395502.
- [26] J. P. Perdew, A. Ruzsinszky, G. I. Csonka, O. A. Vydrov, G. E. Scuseria, L. A. Constantin, X. Zhou, K. Burke 100 (2008) 136406.
- [27] J. Heyd, G. E. Scuseria, M. Ernzerhof, Erratum: Hybrid Functionals Based on a Screened Coulomb Potential [*J. Chem. Phys.* 118, 8207 (2003)], *J. Chem. Phys.* 124 (2006) 219906.
- [28] J. L. F. Da Silva, M. V. Ganduglia-Pirovano, J. Sauer, V. Bayer, G. Kresse, Formation of the cerium orthovanadate CeVO_4 : DFT+U study, *Phys. Rev. B* 75 (2007) 045121.
- [29] B. G. Janesko, T. M. Henderson, G. E. Scuseria, Screened hybrid functionals for solid-state chemistry and physics, *Phys. Chem. Chem. Phys.* 11 (2009) 443.
- [30] C. Freysoldt, B. Grabowski, T. Hickel, J. Neugebauer, G. Kresse, A. Janotti, C. G. Van de Walle, First-principles calculations for point defects in solids, *Rev. Mod. Phys.* 86 (2014) 253–305.
- [31] Y.-H. Kye, C.-J. Yu, U.-G. Jong, K.-C. Ri, J.-S. Kim, S.-H. Choe, S.-N. Hong, S. Li, J. N. Wilson, A. Walsh, Vacancy-Driven Stabilization of the Cubic Perovskite Polymorph of CsPbI_3 , *J. Phys. Chem. C* 123 (2019) 9735–9744.
- [32] D. N. Batchelder, R. O. Simmons, Lattice constants and thermal expansivities of silicon and calcium fluoride between 6°C and 322°C, *J. Chem. Phys.* 41 (1964) 2324–2329.
- [33] G. W. Rubloff, Far-ultraviolet reflectance spectra and the electronic structure of ionic crystals, *Phys. Rev. B.* 5 (1972) 662–684.
- [34] M. L. Agiorgousis, Y.-Y. Sun, H. Zeng, S. Zhang, Strong Covalency-Induced Recombination Centers in Perovskite Solar Cell Material $\text{CH}_3\text{NH}_3\text{PbI}_3$, *J. Am. Chem. Soc.* 136 (2014) 14570–14575.
- [35] A. M. Ibraheem, M. A. Khalafalla, M. H. Eisa, First principle calculation of accurate native defect levels in CaF_2 , *Eur. Phys. J. B* 90 (2017) 40.
- [36] M.-H. Du, Using DFT Methods to Study Activators in Optical Materials, *ECS J. Solid State Sc.* 5(1) (2016) 30073018.